J Electroceram (2009) 23:305–311
DOI 10.1007/s10832-008-9444-z

$FeWO_4Cl$ as cathode material for lithium rechargeable battery

Sookhyeon Im · Jinhee Park · Heesung Oh · Jinho Choy · Claude Delmas · Kyooseung Han

Received: 30 May 2007 / Accepted: 11 February 2008 / Published online: 30 March 2008

Abstract Lithium has been electrochemically and chemically intercalated into layered $FeWO_4Cl$. The discharge curve between $FeWO_4Cl$ and Li_2FeWO_4Cl is constituted by three potential plateaux and two domains where the cell voltage decreases rapidly upon the intercalation of lithium ions. A wide bi-phase domain is obtained for x in Li_xFeWO_4Cl ranging between 0.0 and 0.85. The limit of a solid solution extends in the vicinity of the $LiFeWO_4Cl$ composition. The theoretical and practical discharge capacities for $Li_{1-x}FeWO_4Cl$ are 79.03 mAh/g and 78.45 mAh/g respectively. The structures of $FeWO_4Cl$ and $LiFeWO_4Cl$ were determined: from single crystal analysis and by Rietveld refinement of the powder X-ray diffraction pattern respectively. The modifications of the Fe–O bond lengths emphasize the iron reduction during the discharge process. Moreover, the strong change of Fe–Cl distance suggests a reversible framework modification.

Keywords $FeWO_4Cl$ · Lithium rechargeable battery · Cathode · Intercalation

S. Im · J. Park · H. Oh · K. Han (✉)
Department of Fine Chemical Engineering and Chemistry,
Chungnam National University,
220 Kung,
Youseong, Taejeon 305-764, South Korea
e-mail: kshan@cnu.ac.kr

J. Choy
Department of Chemistry, Ewha Womans University,
Seoul, South Korea

C. Delmas
Institut de Chimie de la Matière Condensée de Bordeaux,
Av. Dr. A. Schweitzer,
33608 Pessac Cedex, France

1 Introduction

Layers of $FeWO_4Cl$ are extended 2-dimensionally by corner sharing of slightly distorted tetrahedral WO_4 and square pyramidal FeO_4Cl [1]. From the view point of atomic position in the $FeWO_4Cl$ unit cell, the lattice can be also described as two layers of chlorine atoms sandwiching the corrugated metal oxygen planes. Due to the open nets of chlorine atoms in the basal plane, adjacent layers could interpenetrate each other and consequently each chlorine atom dips into the cavity formed by four oxygen atoms of the basal FeO_4Cl plane in a neighboring layer. The chemical bonding nature between adjacent layers is considered to be mainly Van der Waals type but partially iono-covalent. Consequently, it is thought that $FeWO_4Cl$ can be one of the host candidates for intercalating guest molecules or ions into its two dimensional lattice, and at the same time, its intercalation chemistry might provide a better understanding for its peculiar interlayer nature. In this paper, lithium ion intercalation into $FeWO_4Cl$ has been undertaken. The structural modifications induced by lithium ion intercalation are presented.

2 Experimental

$FeWO_4Cl$ was obtained from WO_3, Fe_2O_3 and $FeC1_3$ in the molar ratio (3: 1: 1.05). Iron trichloride acts as a reactant but also as a transport agent. The reaction is performed in a sealed evacuated silica tribe at 420°C for 7 days. In this chemical vapor transport technique, large single crystals of $FeWO_4Cl$, up to 4×4×1 mm in size, are obtained in the cold zone of the tube with a very low yield. It must be noted that all experiments realized to obtain $FeWO_4Cl$ by direct synthesis

as a powder form failed. Therefore, only a very small amount of the starting material ($FeWO_4Cl$) was available for the chemical and electrochemical characterizations.

Single crystal structure determination was performed on an Enraf-Nonius CAD4 X-ray diffractometer after a preliminary study with the Weissenberg and Buerger techniques.

Chemical lithium intercalation was realized by action of an excess of LiI in CH_3CN.

Electrochemical lithium intercalation/deintercalation experiments were performed in small lithium rechargeable batteries using a 1 M solution of $LiClO_4$ in propylene carbonate as electrolyte and a mixture of the studied material powder with ketjenblack (35% in weight) as positive electrode. The thermodynamic electrochemical curves were obtained by alternating discharge (or charge) and relaxation periods. The relaxation was considered as finished when the slope of the $V=f(t)$ curve was smaller than 0.1 mV/h.

For the intercalated material, the structure was determined from powder data using the Rietveld method (Fullprof program [2]).

3 Crystal structure of $FeWO_4Cl$

A single crystal exhibiting a truncated rectangular habit {−110} with dimensions 150×200×30 μm was selected for collection of the intensities. A preliminary films study (Weissenberg, Buerger) confirmed the tetragonal symmetry with the Laue group 4/mmm. The systematic absences observed ($h+k=2n+1$ for ($hk0$)) are compatible with the P4/nmm space group. The experimental conditions used for the diffracted intensity collection are reported in Table 1.

The observed intensities were treated for Lorentz polarization effects and an analytical correction for absorption using the shape and dimensions of the crystal was done. This absorption correction is important because of the platelet habit and the high value of the linear absorption coefficient (28.6 mm^{-1}). The transmission coefficient ranges from 0.073 to 0.444: Table 1 indicates the evolution of the coherence factor (R_{int}: 0.083 before absorption correction; 0.033 after absorption correction).

Atomic diffusion factors of W^0, Fe^{3+}, Cl^-, O^- have been corrected for anomalous dispersion. The correction terms $\Delta f'$ and $\Delta f''$ were taken in International Tables.

The structure was solved using the SHELX 76 program, with the heavy atom method. The W coordinates obtained in the powder structural determination of $FeWO_4Cl$ were utilized as a starting hypothesis [1]. The successive Fourier difference functions confirm the sites found for the Fe, Cl, O atoms. The refinement with individual isotropic thermal parameters for all of the atoms converged to a relatively high

Table 1 Experimental conditions for the $FeWO_4Cl$ single crystal structure determination and refinement results.

Single crystal	
Space group	P4/nmm ($N°=129$)
A (Å)	6.677(5)
c (Å)	5.270(5)
V (Å^3)	234.95
D_{cal} (g/cm^3)	4.79
μ (MoKα) (cm^{-1})	285.6
F (000)	298
Collection of intensities	
Temperature	298 K
Crystal size (mm)	0.15×0.20×0.03
Automatic diffractometer	CAD4 Enraf-Nonius
Wave length (Å)	MoKα (λ=0.7107)
Monochromator	Graphite
Scan type	ω
Scan angle (°)	1.00+0.35 tan θ
Counter slit width (mm)	3.00+2.00 tan θ
Angular range	$\theta<45°$
Miller index range	$-13\le h\le 13$
	$-13\le k\le 13$
	$-10\le l\le 10$
Number of the measured intensities	7705
Number of the independent reflections (I>3σ(I))	507
R(INT) before the absorption correction	0.083
R(INT) after the absorption correction	0.033
Collection of intensities	
Number of refined variables	16
Parameter of the secondary extinction	$86(4)\times10^{-4}$
Residuary electron density between W and O (eÅ^{-3})	2.1
Reliability factor	R=0.026
	$Rw(w=1/\sigma^2)$=0.032

R value (R=0.11) with a strong residue of electron density near the tungsten atom (≈7 eÅ^{-3}). An important improvement was obtained when anisotropic thermal parameters were authorized. Final calculation with the weighting scheme

Table 2 Positional and thermal parameters for the atoms of $FeWO_4Cl$.

Atoms	W	Fe	Cl	O
x/a	0.750(0)	0.250(0)	0.250(0)	0.250(0)
y/b	0.250(0)	0.250(0)	0.250(0)	0.964(4)
z/c	0.000(0)	0.275(3)	0.693(9)	0.195(7)
K	0.125(0)	0.125(0)	0.125(0)	0.500(0)
U_{11}	0.005(2)	0.006(5)	0.037(9)	0.019(8)
U_{22}	0.005(2)	0.006(5)	0.037(9)	0.008(2)
U_{33}	0.015(8)	0.010(5)	0.012(7)	0.023(6)
U_{23}	0.000(0)	0.000(0)	0.000(0)	−0.001(8)
U_{13}	0.000(0)	0.000(0)	0.000(0)	0.000(0)
U_{12}	0.000(0)	0.000(0)	0.000(0)	0.000(0)

Table 3 Main interatomic distances in $FeWO_4Cl$ and $LiFeWO_4Cl$.

	Distances (Å)	
	$FeWO_4Cl$	$LiFeWO_4Cl$
Fe–Cl	2.18(6)	2.62(2)
Fe–Cl′	3.03(6)	2.44(3)
Fe–O_1, Fe–O_3	1.93(9)	1.97(4)
Fe–O_2	1.93(9)	2.18(2)
Fe–O_4	1.93(9)	1.94(8)
W–O_1, W–O_3	1.75(1)	1.77(8)
W–O_2	1.75(1)	1.84(4)
W–O_4	1.75(1)	1.80(6)
Li–O_1	–	2.18(8)
Li–O_2	–	2.21(7)
Li–Cl	–	2.63(6)

$w=1/\sigma^2(F_o)$, the x parameter of the secondary extinction correction $\left[F_c = F\left(1 - 10^{-4} \times F^2/\sin\theta\right)\right]$, and anisotropic thermal parameters for all atoms converged to R=0.026 and R_w=0.032 (Table 1). The atomic coordinates are given in Table 2. The main interatomic distance (Å) and angles (°) in $FeWO_4Cl$ are given in Tables 3 and 4.

Figure 1 represents a perspective view of the structure of $FeWO_4Cl$ (CERIUS program). It consists of a packing of $FeWO_4Cl$ layers along the c axis. Iron is in an FeO_4Cl square pyramidal environment. The 4 oxygen atoms also belong to the WO_4 tetrahedra, leading to a puckered slab. The square pyramids alternately point their chlorine atoms up and down. The Fe–Cl distance within a square pyramid is equal to 2.18 Å, this value is considerably smaller than the Fe–Cl′ distance which involves a chlorine atom of the next layer (3.03 Å). If the two distances were not so different, an octahedral environment for iron (FeO_4ClCl') would be considered and the layered character of this structure would be lost.

Table 4 Main interatomic angles in $FeWO_4Cl$ and $LiFeWO_4Cl$.

	Angles (°)	
	$FeWO_4Cl$	$LiFeWO_4Cl$
Cl–Fe–Cl′	180.0(0)	175.0(4)
Cl–Fe–O_1	102.3(8)	89.1(7)
Cl–Fe–O_2	102.3(8)	80.0(1)
Cl–Fe–O_4	102.3(8)	95.8(2)
O_1–W–O_2	109.9(0)	109.2(5)
O_1–W–O_4	109.9(0)	105.0(3)
O_2–W–O_4	108.5(5)	111.7(0)
O_1–Fe–O_2	87.3(5)	83.6(6)
O_1–Fe–O_3	155.2(6)	167.3(0)
Fe–O_2–W	156.6(7)	127.3(6)
Fe–O_4–W	156.6(7)	160.1(8)

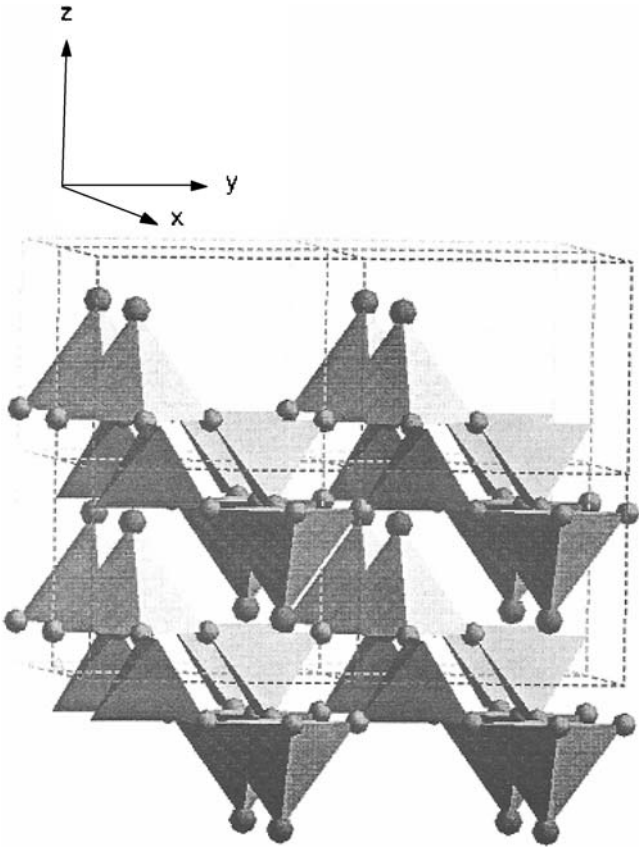

Fig. 1 A perspective view of the structure of $FeWO_4Cl$

4 Lithium intercalation

All experiments were realized on ground powders of $FeWO_4Cl$. All trials to intercalate directly on the single crystals have failed. In the case of chemical intercalation, the reaction of an excess of LiI in CH_3CN on $FeWO_4Cl$ leads to $LiFeWO_4Cl$. This material was characterized by X-ray diffraction. The results are discussed further. This material has been used as the positive electrode of lithium rechargeable batteries in order to compare the electrochem-

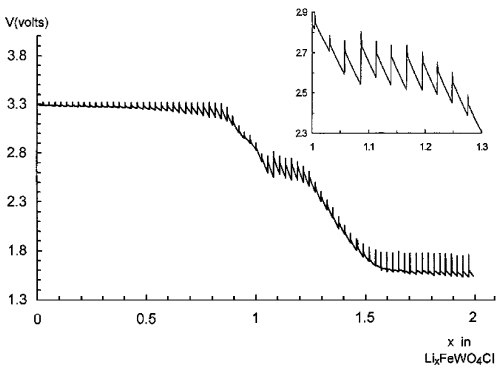

Fig. 2 Variation of the open circuit voltage vs. the amount of intercalated lithium ion (x) during a first discharge to x=2.0 for a Li// $FeWO_4Cl$ cell

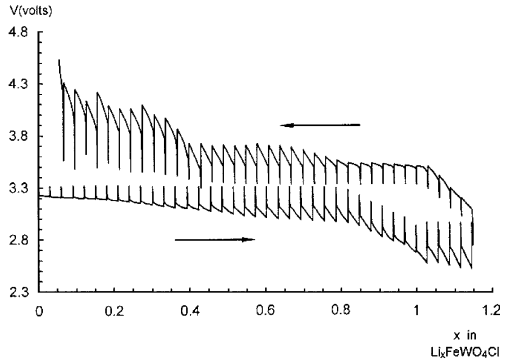

Fig. 3 Variation of the open circuit voltage vs. the x in Li_xFeWO_4Cl during a discharge/charge cycle starting from $FeWO_4Cl$

ical behavior of $FeWO_4Cl$ and of $LiFeWO_4Cl$ obtained chemically.

As only a small amount of $FeWO_4Cl$ starting material was available, only open circuit voltage (OCV) experiments were realized in order to obtain directly the $LiFeWO_4Cl$ phase diagram. Figure 2 gives the variation of the cell voltage vs. the amount of intercalated lithium ion. The discharge curve is constituted by three potential plateaux and two domains where the cell voltage decreases rapidly upon intercalation. A close examination of this curve shows that only the first plateau ($0.00<x<0.85$) corresponds to a true biphased domain between two well identified materials: the OCV is

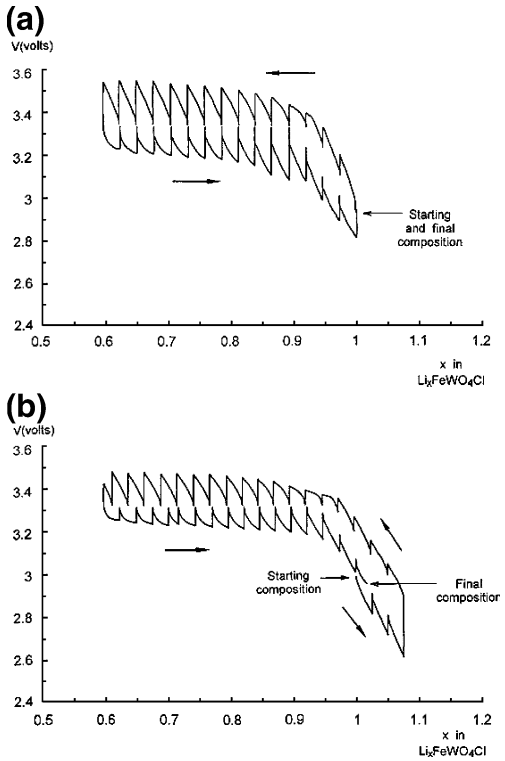

Fig. 4 Variation of the open circuit voltage vs. the x in Li_xFeWO_4Cl during a cycle starting from $LiFeWO_4Cl$ obtained chemically: (**a**) charge and discharge, (**b**) discharge, charge, and discharge

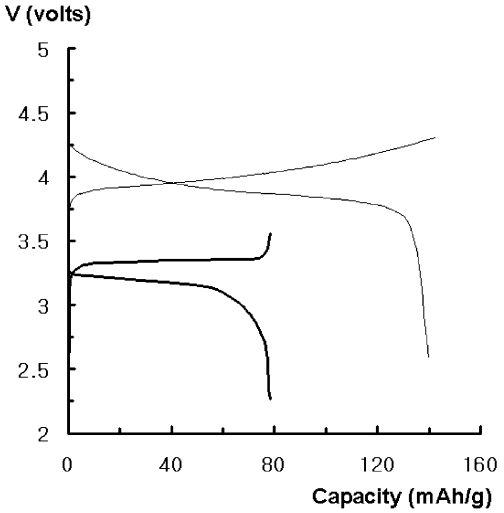

Fig. 5 Cell potential vs. capacity profiles of $LiFeWO_4Cl$ (*thick solid line*) and $LiCoO_2$ (*thin solid line*)

absolutely constant in all involved composition domain. On the contrary for the other two plateaux, the OCV values vary slightly from one composition to the next one indicating the occurrence of some irreversible process. For the last plateau, this point is confirmed by the X-ray diffraction study of the material obtained after intercalation of two lithium ions which indicates a mixture of $LiFeWO_4Cl$ with an amorphous phase. As a result, in the following of this study, our attention has been specially focused on the intercalation of the first lithium ion.

As shown in Fig. 3, the first lithium ion can be deintercalated with a relatively small hysteresis effect. The wide potential plateau is characteristic of a biphased domain between the $FeWO_4Cl$ composition and a composition close to $Li_{0.85}FeWO_4C1$ (Fig. 2). The latter can be considered as the lower limit of a solid solution which extends in the vicinity of the $LiFeWO_4Cl$ composition. In order to have a better characterization of the extent of this solid solution, two cells, using the $LiFeWO_4Cl$ phase obtained chemically by action of LiI on $FeWO_4Cl$, were built. Both of them have been cycled in OCV conditions around the starting composition. The cycling curves are shown In Fig. 4. In order to suppress the irreversible processes shown in discharge when the cell voltage becomes smaller than 2.55 V, the end of discharge has been limited to 2.60 V. Under these conditions the reversibility is very good. The solid solution around the

Table 5 Lattice parameters for $FeWO_4Cl$ and $LiFeWO_4Cl$.

Unit cell parameters	a (Å)	b (Å)	c (Å)	β (°)
$FeWO_4Cl$	6.631(9)	6.631(9)	5.223(9)	90.0(0)
$LiFeWO_4Cl$	7.071(3)	6.947(1)	5.060(0)	91.5(2)

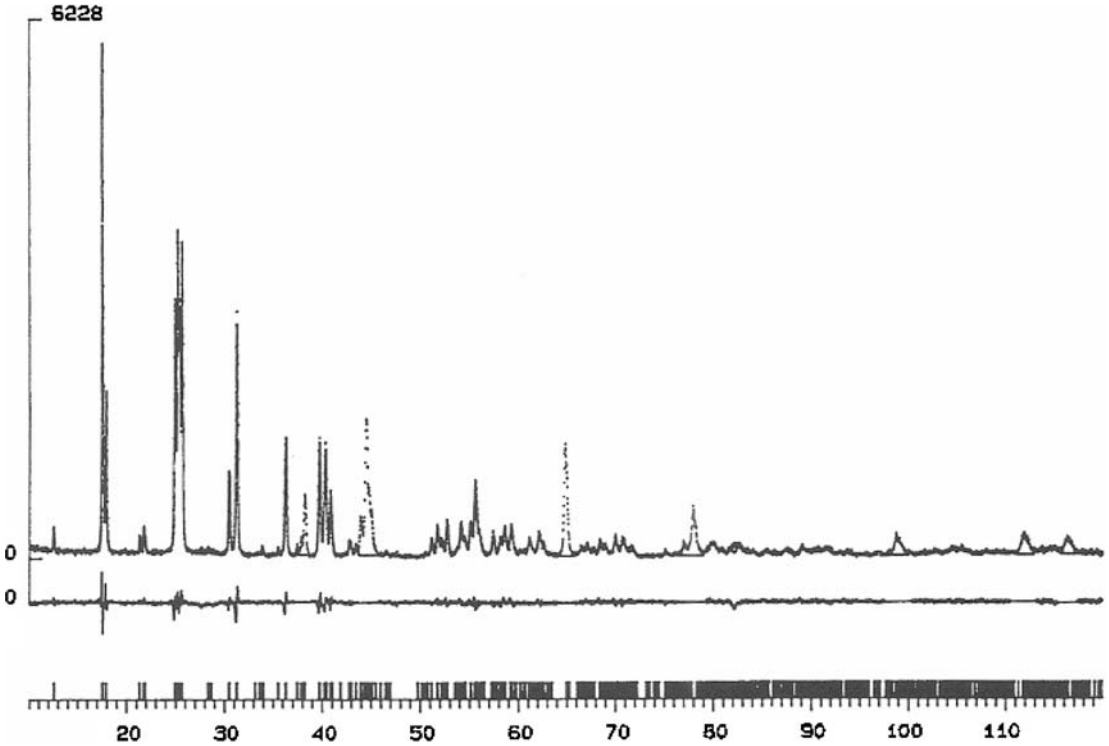

Fig. 6 X-ray powder diffraction profile and difference between observed and calculated intensities for $LiFeWO_4Cl$

$LiFeWO_4Cl$ composition extends in the range $0.90<x<1.07$. These values must be compared to those found during the lithium intercalation into $FeWO_4Cl$ (Fig. 2; $0.85<x<1.05$). The very small discrepancy between the two limits can result from a slight inaccuracy in the weight of the $FeWO_4Cl$ phase within the cell and/or the starting composition considered for the material obtained by chemical intercalation with LiI. There is no reason why this composition should be exactly $LiFeWO_4Cl$. As a solid solution exits, the true composition is fixed by the equilibrium in potential between the $I°/I^-$ redox couple and Li_xFeWO_4Cl.

Owing to a small amount of $FeWO_4Cl$, another lithium cell could be realized from $LiFeWO_4Cl$ obtained chemically using LiI in CH_3CN on $FeWO_4Cl$. As shown in Fig. 5, the material exhibits the discharge capacity of 78.45 mAh/g with the current density of 30 $\mu A/cm^2$. The discharge capacity of the material is evidently poor in comparison with that of $LiCoO_2$ as the cathode material for almost all commercialized lithium rechargeable batteries. Considering the theoretically feasible discharge capacity of 79.03 mAh/g for $Li_{1-x}FeWO_4Cl$ ($0\leq x\leq 1$) phase, the practical discharge capacity of 78.45 mAh/g indicates that almost one mole of lithium ion can be intercalated and deintercalated into $FeWO_4Cl$.

The existence of a large biphased system between the two end members may result from the important structural modifications imposed by the lithium intercalation. It must be noticed that any solid solution in the vicinity of the $FeWO_4Cl$ composition cannot be detected. This result shows that the iron reduction leads immediately to the nucleation of the Li_xFeWO_4Cl phase ($x\approx 1$). As the structure of the unintercalated material was known precisely from a single crystal study, a structural study using the

Table 6 Positional and isotropic thermal parameters for the atoms of $LiFeWO_4Cl$.

Atoms	*x*/*a*	*y*/*b*	*z*/*c*	*K*	*B* (Å^2)
W	0.736(9)	0.250(0)	0.998(3)	1.000(0)	1.1
Fe	0.246(7)	0.250(0)	0.181(0)	1.000(0)	0.7
Cl	0.262(2)	0.250(0)	0.699(3)	1.000(0)	1.8
O_1	0.277(5)	0.967(6)	0.186(0)	2.000(0)	2.2
O_2	0.552(7)	0.250(0)	0.249(3)	1.000(0)	1.0
O_4	0.971(6)	0.250(0)	0.147(8)	1.000(0)	1.3
Li	0.500(0)	0.000(0)	0.500(0)	1.000(0)	1.9

Rietveld refinement method was carried out on the $LiFeWO_4Cl$ phase obtained after the electrochemical cycle represented in Fig. 4(a).

While the $FeWO_4Cl$ phase crystallizes in the tetragonal system, the $LiFeWO_4Cl$ phase crystallizes in the monoclinic system. The unit cell parameters of the $LiFeWO_4Cl$ phase are reported in Table 5. This lowering in symmetry may indicate an ordered occupancy by lithium of part of the available sites within the structure.

An X-ray diffraction pattern of the electrode material corresponding to the $LiFeWO_4Cl$ composition was carefully recorded (step of 0.02° (2θ)/40 s counting time). As the material amount was quite small, the lines of the aluminum sample holder appear on the diffraction pattern. Regions of the scan which include these diffraction peaks were excluded for the refinement. The background was determined by using a polynomial function. The reliability factors obtained after the fits were R_I=0.056, R_{wp}=0.171. Figure 6 gives the observed and calculated X-ray diffraction patterns and the difference between them. The R values, although not very good due to the difficult experimental conditions imposed by the study of an electrode material, can be considered with interest for the structure discussion. The atomic positions are reported in Table 6, while the main interatomic distances and angles are reported in Tables 3 and 4 in comparison with those of the starting material. The Rietveld refinement does not allow to fit the lithium positions, therefore those determined by Torardi et al. for $LiFeMoO_4Cl$ in the neutron diffraction study have been used [3].

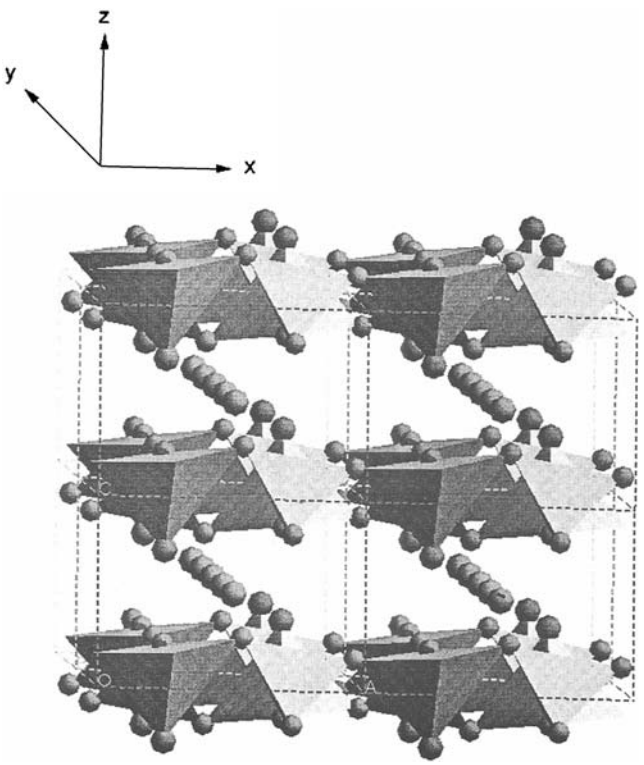

Fig. 7 A perspective view of the structure of $LiFeWO_4Cl$

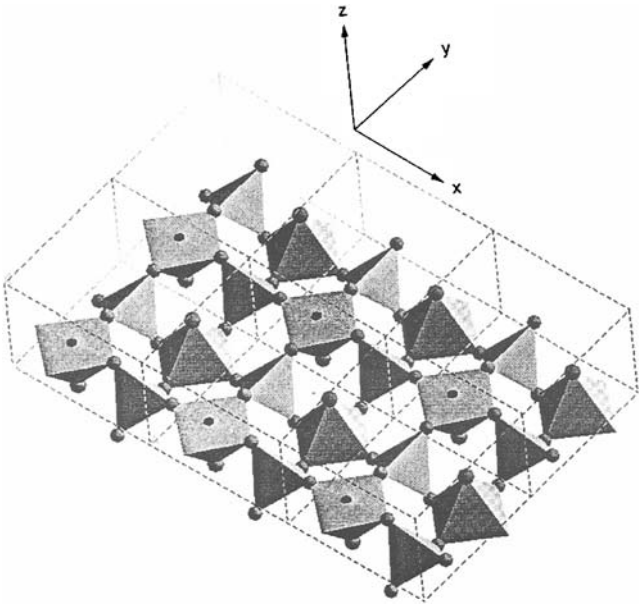

Fig. 8 A perspective view of one layer in $LiFeWO_4Cl$

A perspective representation of the overall structure is given in Fig. 7. A view of one slab is represented (in Fig. 8) perpendicularly to the previous figure. The structural change between the pristine $FeWO_4Cl$ phase (Fig. 1) and the $LiFeWO_4Cl$ phase shows that the polyhedra around iron ions are strongly modified. In fact, during the reduction, the Fe–Cl distance within the FeO_4Cl square pyramid increases considerably. It follows that the structural representation privileges an FeO_4Cl' square pyramidal environment instead of an FeO_4ClCl' distorted octahedral one. These structural modifications upon lithium intercalation are schematically represented in Fig. 9. The distortion of the octahedra is quite strong and the structure of $LiFeWO_4Cl$ can rather be considered as being bidimensional. This behavior is illustrated be the larger value of the c parameter: the larger the 2D character, the weaker the interslab bonds and the larger the interslab distance.

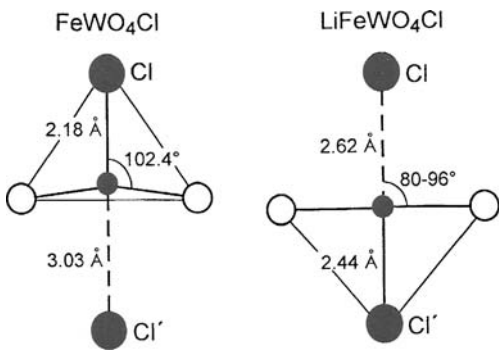

Fig. 9 Schematic representations of the main structural modifications upon lithium ion intercalation in $FeWO_4Cl$

The increase of the Fe–O distances (Tables 3 and 4) shows that iron is reduced to the divalent state upon intercalation, this reduction leads to an increase of the basal distances ($a_{mon.}$ and $b_{mon.}$) as shown in Table 4. On the contrary, the lithium intercalation entails a contraction of the interslab space as illustrated by the strong decrease of the c parameter.

Reference

1. J.H. Choy, D.Y. Noh, H.H. Park, J.C. Park, J. Chem. Soc. Dalton Trans. **1647** (1991)
2. J. Rodriguez-Carvajal, Collected Abstracts of Powder Diffraction Meeting, France **127** (1990)
3. C.C. Torardi, W.M. Reiff, K. Lazar, E. Prince, J. Phys. Chem. Solids **47**(8), 741 (1986)